GAP, an aequorin-based fluorescent indicator for imaging Ca^{2+} in organelles

Arancha Rodriguez-Garcia, Jonathan Rojo-Ruiz, Paloma Navas-Navarro, Francisco Javier Aulestia, Sonia Gallego-Sandin, Javier Garcia-Sancho, and Maria Teresa Alonso[1]

Instituto de Biología y Genética Molecular (IBGM), Universidad de Valladolid and Consejo Superior de Investigaciones Científicas, 47003 Valladolid, Spain

Edited by Ramon Latorre, Centro Interdisciplinario de Neurociencias, Universidad de Valparaíso, Valparaíso, Chile, and approved January 2, 2014 (received for review September 4, 2013)

Genetically encoded calcium indicators allow monitoring subcellular Ca^{2+} signals inside organelles. Most genetically encoded calcium indicators are fusions of endogenous calcium-binding proteins whose functionality in vivo may be perturbed by competition with cellular partners. We describe here a novel family of fluorescent Ca^{2+} sensors based on the fusion of two *Aequorea victoria* proteins, GFP and apo-aequorin (GAP). GAP exhibited a unique combination of features: dual-excitation ratiometric imaging, high dynamic range, good signal-to-noise ratio, insensitivity to pH and Mg^{2+}, tunable Ca^{2+} affinity, uncomplicated calibration, and targetability to five distinct organelles. Moreover, transgenic mice for endoplasmic reticulum-targeted GAP exhibited a robust long-term expression that correlated well with its reproducible performance in various neural tissues. This biosensor fills a gap in the actual repertoire of Ca^{2+} indicators for organelles and becomes a valuable tool for in vivo Ca^{2+} imaging applications.

calcium signalling | Golgi apparatus | hippocampus | motor neuron

Ca^{2+} is involved in the regulation of many intracellular processes that take place both in the cytosol and inside organelles (1–3). Therefore, accurate measurement of the calcium concentration ($[Ca^{2+}]$) inside organelles is essential to discriminate discrete Ca^{2+} signals between the different compartments. Although synthetic Ca^{2+} indicators can be loaded into organelles, the signal has poor selectivity, as the dye is also present in the cytosol and must be carefully removed before measurements (4). The main advantage of Genetically Encoded Ca^{2+} Indicators (GECIs) is their ability to be targeted to specific intracellular locations. Both bioluminescent and fluorescent proteins have been successfully used to measure subcellular $[Ca^{2+}]$. The photoprotein aequorin (5), purified from the jellyfish *Aequorea victoria*, was the first protein-based Ca^{2+} indicator, injected into cells in the early 1970s (6). After cloning of its cDNA (7), recombinant aequorin became the most frequently used probe to measure Ca^{2+} in organelles, including mitochondria (8), the endoplasmic reticulum (ER) (9), the nucleus (10), the Golgi apparatus (11), or secretory vesicles (12).

Fluorescent GECIs achieve a better spatial resolution than bioluminescent sensors. They are generally composed of one or two fluorescent proteins, most of them variants of GFP, fused to a Ca^{2+}-binding protein (13). Recently, a single EF-hand motif has been inserted in the GFP moiety to generate a Ca^{2+} fluorescent probe (14). Since the first cameleon based on FRET (15), the number of GECIs has exponentially increased, attempting optimization of critical features such as adequate expression, signal strength, or dynamic range. However, the in vivo use in mammals, one of the main applications of GECIs, has grown more slowly and has disclosed severe limitations (16, 17). Transgenic sensors usually showed a low expression, often resulting in its inactivation or reduced dynamic range. With the exception of troponin derivatives, most of the available GECIs, namely cameleons, camgaroos, pericams, or GCaMPs (circularly permutated EGFP-based Ca^{2+} sensors), are based on calmodulin, a highly regulated ubiquitous protein that binds a large number of targets (13). Although the interference with endogenous calmodulin has been reduced in the improved cameleons (18), the interaction with other cellular proteins cannot be ruled out. Thus, the loss of Ca^{2+} sensitivity observed in vivo may reflect the interaction of the probe with endogenous partners, which may disturb cellular functions.

The jellyfish aequorin exhibits a number of advantages over mammalian EF-hand proteins. It is not toxic and appears not to interfere with other intracellular Ca^{2+}-binding molecules, even when microinjected at high concentrations in mammalian cells. Moreover, the use of aequorin as a bioluminescence sensor has been extensively reported, ranging from subcellular Ca^{2+} measurements in many different cell types up to whole organisms, including transgenic animals (19–21).

Here we describe a family of fluorescent Ca^{2+} sensors based on the fusion of two jellyfish proteins, GFP and apoaequorin. This Ca^{2+} probe shows a larger dynamic range compared with other GECIs and a robust photonic and thermal stability. It can be targeted to distinct compartments such as the nucleus, cytosol, or mitochondria, where it selectively and accurately monitors dynamic Ca^{2+} changes. In addition, we have generated a variant with a lower Ca^{2+} affinity suited for imaging Ca^{2+} changes in organelles with high resting $[Ca^{2+}]$ such as the ER or the Golgi apparatus. Finally, we demonstrate its in vivo applicability by generating transgenic mice where the Ca^{2+} biosensor maintained its in vitro features.

Results

Development and Characterization of GAP Ca^{2+} Indicator. We have previously engineered calcium probes by fusing various fluorescent proteins to apoaequorin that, upon reconstitution with its

Significance

Genetically encoded calcium indicators are excellent tools to monitor subcellular Ca^{2+} signals inside organelles. We describe here a novel family of fluorescent Ca^{2+} sensors based on the fusion of an improved GFP variant and aequorin, named GFP–Aequorin Protein (GAP). Since GFP and aequorin are both from jellyfish, with no mammalian homologues, the possibility of interactions between GAP and mammalian partners is minimized. This makes GAP a truly orthogonal calcium indicator in contrast to the widely used calmodulin-based indicators. GAP displays many advantages over other existing Ca^{2+} probes, including its ability to be targeted to multiple organelles and its functionality in vivo. This Ca^{2+} biosensor opens an avenue for studies of Ca^{2+} dynamics in vivo.

Author contributions: J.G.-S. and M.T.A. designed research; A.R.-G., J.R.-R., P.N.-N., F.J.A., and S.G.-S. performed research; A.R.-G., J.R.-R., P.N.-N., F.J.A., S.G.-S., J.G.-S., and M.T.A. analyzed data; and J.G.-S. and M.T.A. wrote the paper.

The authors declare no conflict of interest.

This article is a PNAS Direct Submission.

[1]To whom correspondence should be addressed. E-mail: talonso@ibgm.uva.es.

This article contains supporting information online at www.pnas.org/lookup/suppl/doi:10.1073/pnas.1316539111/-/DCSupplemental.

cofactor celenterazine, emitted bioluminescence (22). Interestingly, some of the GFP fusions without the cofactor exhibited Ca^{2+}-dependent fluorescence, and hence could potentially be used as fluorescent Ca^{2+} probes. Fusing GFP directly to the *N* terminus of aequorin resulted in a protein with no response to Ca^{2+}. We thus inserted a spacer between the two protein moieties, varying its length by 9, 16, or 32 residues (a tandem repeat of a 16-mer linker). The chimeric protein consisting of a GFP variant (23) (Q80R, F99S, M153T, V163A) fused to the N terminus of apoaequorin via a 16-residue linker (24) exhibited Ca^{2+} sensitivity (Fig. 1*A*). We dubbed this GECI family GFP–Aequorin Protein (GAP). A hexahistidine tail was attached to its N terminus to facilitate purification. When expressed in *Escherichia coli*, a 50-kDa protein was produced, as predicted from its theoretical molecular weight (Fig. 1*B*).

The excitation spectrum of GAP maintained the two peaks of wtGFP, at 403 and 470 nm, and it was sensitive to Ca^{2+} (Fig. 1*C*). The Ca^{2+}-free protein exhibited a major 403-nm peak and a minor shoulder at 470 nm, whereas the Ca^{2+}-saturated protein showed a dominant 470-nm peak with a small shoulder at 403 nm. The emission spectrum showed a single maximum at 510 nm, which was not shifted by addition of Ca^{2+}. Ca^{2+} calibration demonstrated a dynamic range of ~three- to fourfold in the F_{470}/F_{403} ratio (Fig. 1*D*). The data fitted to a Michaelis function with an apparent K_d for Ca^{2+} of 200 nM, a value well suited for Ca^{2+} measurements in the cytosol, and a Hill coefficient of 1. The calibration assay was performed in the presence of 1 mM Mg^{2+} and was not modified in the 0.2–5 mM Mg^{2+} range, demonstrating a good selectivity for Ca^{2+} over Mg^{2+} (Fig. S1*A*).

To explore the performance of GAP in living cells, we cloned its cDNA into an eukaryotic expression vector (Fig. 1*A*) and transfected HeLa or HEK293 cells. GAP fluorescence was distributed homogeneously in both cytosol and nucleus with no signs of aggregation, and the F_{470}/F_{403} ratio changed as predicted with stimuli designed to modify $[Ca^{2+}]_C$. In GAP-expressing HeLa cells, maximal stimulation with either ATP (100 μM) or histamine (100 μM), two well-known $InsP_3$-generating stimuli in these cells, increased F_{470} and conversely decreased F_{403} resulting in a twofold F_{470}/F_{403} ratio increase (Fig. 1*E*). In addition, submaximal stimulation (2 μM ATP) generated $[Ca^{2+}]_C$ oscillations that could easily be detected by GAP, indicating its high sensitivity. Reproducible $[Ca^{2+}]_C$ transients in GAP-expressing HEK293 cells stimulated, either with ATP or in response to store-operated Ca^{2+} entry (SOCE) activation, were also observed (Fig. S2). We conclude that GAP fluorescence changes in living cells validating its performance in vitro and demonstrating its utility to monitor intracellular Ca^{2+} dynamics.

GAP Is Targetable to a Variety of Organelles. To test the ability of GAP to monitor subcellular Ca^{2+} dynamics, we targeted it to distinct compartments. Expression in the cytosol, the nucleus, or mitochondria was achieved by using the specific targeting sequences previously reported for aequorin (22, 25) (Fig. 2*A*). Correct targeting was confirmed both by the expression of GFP fluorescence and its colocalization with organelle markers, as well as by functional responses to protocols known to modify $[Ca^{2+}]$ in each particular location (Fig. 2 *B–E*). Maximal stimulation with ATP plus carbachol, which released Ca^{2+} from the ER, increased both $[Ca^{2+}]_C$ (Fig. 2*B*) and nuclear Ca^{2+} concentration ($[Ca^{2+}]_N$) (Fig. 2*C*) to a similar extent, consistent with Ca^{2+} diffusion from cytosol to nucleus (26). Extracellular Ca^{2+} removal hardly modified $[Ca^{2+}]_N$ increase (Fig. 2*C*), as expected

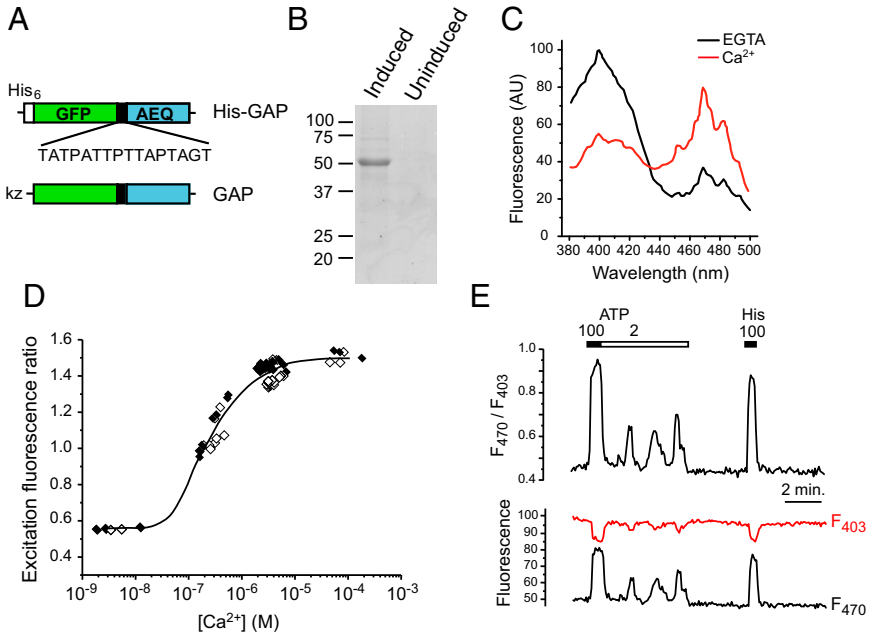

Fig. 1. Development and properties of GAP Ca^{2+} indicators. (*A*) Domain structure of GAP variants used either for expression in bacteria, as a fusion with a polyhistidine tail (His–GAP), or in mammalian cells (GAP). Linker sequence inserted between GFP and apoaequorin (AEQ) is shown; kz, Kozak consensus sequence for optimal expression in mammalian cells. (*B*) SDS/PAGE of recombinant GAP purified from induced and control (uninduced) *E. coli*. (*C*) Fluorescence excitation spectra of GAP (emission, 510 nm) in the presence of 1 mM $CaCl_2$ or in Ca^{2+}-free medium (0.1 mM EGTA). Measurements were performed in saline solution containing 140 mM KCl, 1 mM $MgCl_2$, and 20 mM MOPS–Tris, pH 7.2. (*D*) Ca^{2+} calibration curve of GAP. The excitation fluorescence ratio (F_{485}/F_{390}, equivalent to F_{470}/F_{403}) is represented as a function of $[Ca^{2+}]$. The Ca^{2+} concentrations shown in the abscissa were achieved using calcium/EGTA buffers for concentrations < 10^{-6} M free Ca^{2+}, or unbuffered Ca^{2+} for concentrations > 10^{-6} M. The free Ca^{2+} in each sample was measured simultaneously using X-Rhod-5F (K_d = 1.6 μM). Each sample was measured with 3 μg protein in a microplate fluorescence reader excited at 390 and 485 nm (emission at 535 nm) for GAP and at 535 nm (emission at 590 nm) for X-Rhod-5F. Each data point represents the average of triplicate values combining two independent experiments (open and filled squares). The fitted curve corresponds to the constants given in the text. (*E*) $[Ca^{2+}]_i$ responses in GAP-transfected HeLa cells stimulated with either ATP (100 μM or 2 μM) or histamine (His, 100 μM).

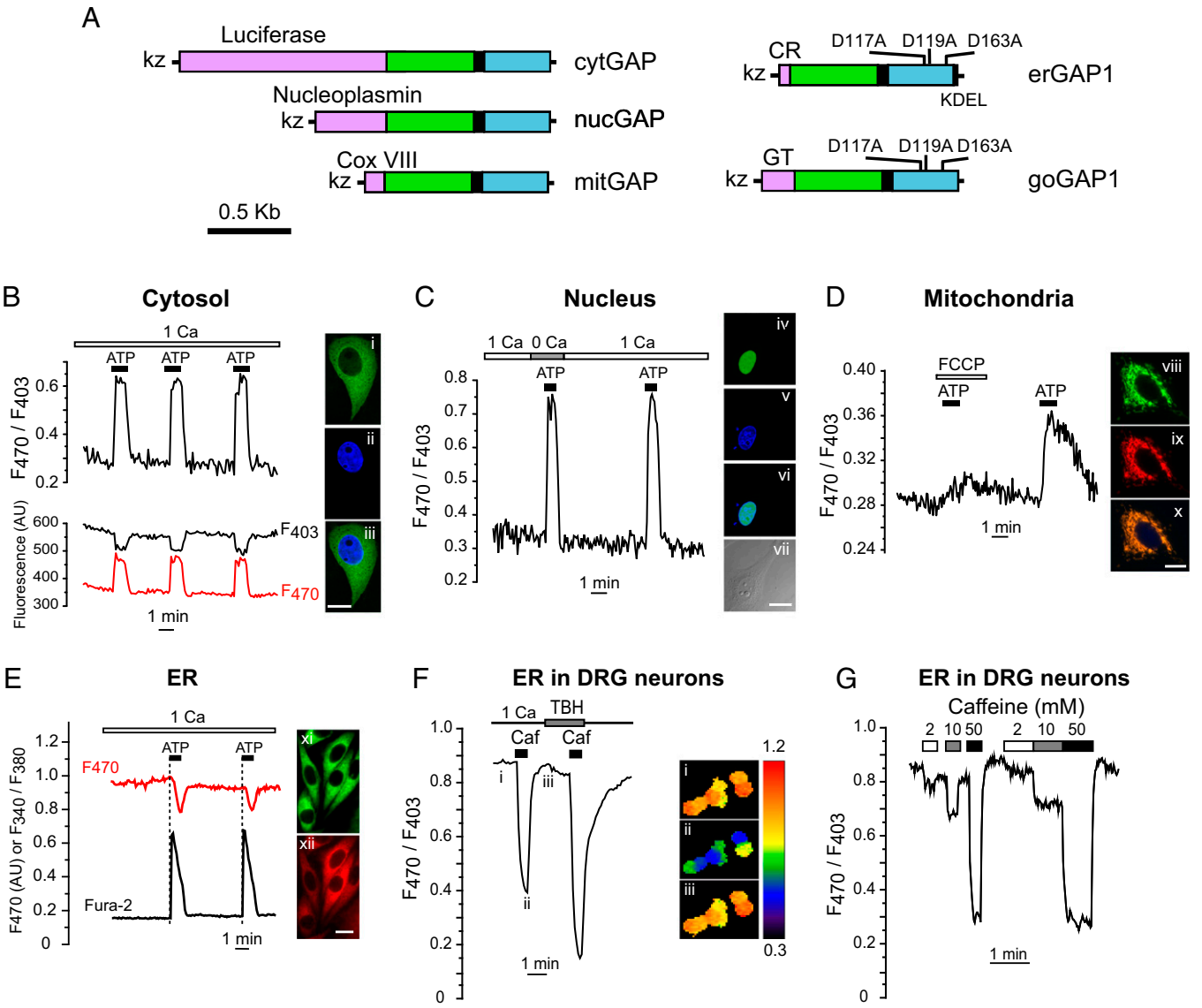

Fig. 2. Functional targeting of GAP to various organelles. (*A*) Domain structure of GAP constructs. CR, calreticulin signal sequence; KDEL, ER retention signal; Cox VIII, cytochrome *c* oxidase VIII; GT, galactosyltransferase II. (*B*) cytGAP–HeLa cells ($n = 5$) stimulated with ATP + carbachol (marked as ATP, 100 μM each). At right, cytGAP–HeLa cell (*i*), (DAPI) (*ii*), and merged image (*iii*). (*C*) nucGAP–HeLa cells ($n = 8$) stimulated with ATP + carbachol (100 μM each one) in 1 mM $CaCl_2$ (1 Ca) or 0.2 mM EGTA (0 Ca). nucGAP (*iv*), DAPI (*v*), merged image (*vi*), and matched phase contrast image (*vii*). (*D*) Changes of the F_{470}/F_{403} ratio in a representative HeLa cell expressing mitochondrial GAP (mitGAP) and stimulated with ATP + carbachol (marked as ATP) in the presence or the absence of the mitochondrial uncoupler FCCP (2 μM). mitGAP (green, *viii*) cotransfected with DsRed2–mt (red, *ix*) and merged image (*x*). (*E*) Simultaneous imaging of cytosolic Ca^{2+} (fura-2, Ratio 340/380) and ER Ca^{2+} (erGAP1, F_{470}) in a representative HeLa cell. Stably expressing erGAP1 HeLa cells (*xi*, green), immunostained with anti-SERCA2b antibody (*xii*, red). (Scale bar for all images *i*–*xii*, 10 μm.) (*F* and *G*) ER Ca^{2+} dynamics in erGAP1 virally transduced DRG neurons. (*F*) Caffeine (20 mM) in 1 mM $CaCl_2$ or 0.2 mM EGTA with SERCA-ATPase inhibitor TBH (10 μM). Trace is the average of the seven cells shown on the *Right* (ratio images coded in pseudocolor). The images (*i*–*iii*) correspond to the time points marked in the trace. See also Movie S1. (*G*) Caffeine dose–response traces of $[Ca^{2+}]_{ER}$.

from stimuli known to release Ca^{2+} from the intracellular stores. The ATP challenge also provoked a transient increase in the mitochondrial Ca^{2+} ($[Ca^{2+}]_M$), which was reversibly prevented by mitochondrial depolarization with trifluorocarbonylcyanide-phenylhydrazone (FCCP) (Fig. 2*D*).

We next focused on the expression of GAP in the ER, where available Ca^{2+} indicators pose serious limitations, namely a small dynamic range (D1ER) (27) or not being ratiometric (catchER) (14). As $[Ca^{2+}]$ inside ER ($[Ca^{2+}]_{ER}$) is higher than $[Ca^{2+}]_C$, we modified GAP to reduce its affinity for Ca^{2+}. A small library of GAP mutants was generated by site-directed mutagenesis at most of the acidic residues of the three functional EF-hand motifs in the aequorin moiety (Fig. S3*A*). The mutant with the best performance, named GAP1, contained the substitutions D117A, D119A, and D163A. The ER-targeting construct, erGAP1, combined the calreticulin signal peptide and the KDEL ER retention sequence, tagged to the *N* and *C* terminus of GAP, respectively (28) (Fig. 2*A*). We then generated a clonal HeLa cell line that stably expressed erGAP1 to facilitate Ca^{2+} calibration in situ (Fig. S3*B*). Collected data fitted to a Hill equation with a coefficient (n) of 1 and a K_d value of 12 μM (Fig. S3*C*). Importantly, despite the 60-fold reduced Ca^{2+} affinity, erGAP1 maintained the dynamic range of GAP (fourfold). The insensitivity to Mg^{2+} shown for GAP was also retained for the low-affinity mutant erGAP1 (Fig. S1*B*). The sensor signal was robust and displayed a typical ER distribution pattern, excluded from the

nucleus and colocalized with the sarco-endoplasmic reticulum ATPase (SERCA) (Fig. 2*E*) and ER tracker. erGAP1 detected ER Ca^{2+} release stimulated by ATP + carbachol, which produced a transient decrease in the ratio of about 20%. Treatment of HeLa cells with the SERCA inhibitor tert-butyl-hydroquinone (TBH), which prevented ER Ca^{2+} reuptake, caused an 80% ratio decrease (Fig. S4*A*). A similar result was obtained by loading the cells with the Ca^{2+} chelator 1,2-bis(o-aminophenoxy)ethane-N,N,N′,N′-tetraacetic acid (BAPTA), which prevented $[Ca^{2+}]_C$ increase at the cytosolic mouth of the $InsP_3R$ (Fig. S4*B*). These data indicate that ER reuptake of cytosolic Ca^{2+} together with inhibition of $InsP_3R$ by Ca^{2+} strongly counteract ER Ca^{2+} release in HeLa cells (29).

Due to nonoverlapping spectra, erGAP1 can be used in combination with fura-2 to simultaneously monitor $[Ca^{2+}]_{ER}$ and $[Ca^{2+}]_C$. In this case, erGAP1 signal was recorded at 470 nm, and fura-2 was recorded at 340 and 380 nm. Two consecutive ATP + carbachol stimuli produced reproducible drops in $[Ca^{2+}]_{ER}$ which coincided with rises in $[Ca^{2+}]_C$ (Fig. 2*E*). The Ca^{2+} probe can also be delivered to neurons by infecting primary cultures with an erGAP1-viral vector. Fig. 2 *F* and *G* illustrates erGAP1 responses to caffeine, which is known to mobilize Ca^{2+} in dorsal root ganglion (DRG) neurons. A maximal dose of caffeine provoked a dramatic and fully reversible release of ER Ca^{2+} (Movie S1). Additional evidence for erGAP1 sensitivity is provided by the caffeine dose–response effect (Fig. 2*G*).

We compared the performance of erGAP1 to that obtained with two other ER sensors, namely catchER (14) or D1ER (27), in two cell types under identical experimental conditions. In HeLa cells, stimulation with ATP + histamine produced a 14.4 ± 2.1% ($n = 7$) ratio change for D1ER in comparison with 58.8 ± 7.5% ($n = 28$) for erGAP1 (Fig. S5). CatchER fluorescence was so dim that we were unable to demonstrate significant Ca^{2+}-sensitive fluorescence changes. We also expressed erGAP1 and D1ER in hippocampal neurons. Upon stimulation with acetylcholine + ATP (and in the presence of 10 μM TBH to avoid ER reuptake), D1ER showed a change of 17.3 ± 1.6 ($n = 8$) versus 48.2 ± 7.4% ($n = 8$) for erGAP1. Therefore, erGAP1 showed a three- to fourfold larger ratio change than that of D1ER.

We next aimed to image Ca^{2+} dynamics in the Golgi apparatus. Because this organelle has a pH of about 6.5, we first checked the pH sensitivity of GAP1. The pH titration measurements showed that GAP1 was mildly sensitive to pH in the 6.2–8.2 range (Fig. S6). The selective targeting to the trans-Golgi apparatus was achieved by fusing GAP1 to human galactosyltransferase II (30), generating goGAP1 (Fig. 2*A*). Expression analysis of goGAP1 fluorescence in a stably expressing HeLa cell line showed a characteristic juxtanuclear punctate-staining pattern that colocalized with the trans-Golgi network (TGN) marker, TGN46 (Fig. S7*A*). The goGAP1 probe reported $[Ca^{2+}]_{GO}$ changes upon stimulation with $InsP_3$-producing agonists (ATP + histamine), which caused a reproducible and reversible decrease of the F_{470}/F_{403} ratio (Fig. S7 *B* and *C*). Taken together, our results demonstrate the ability of GAP to monitor Ca^{2+} dynamics in a variety of organelles using the corresponding targeted GAP.

Transgenic Mice Expressing erGAP1. To investigate whether GAP was functional in living organisms, we generated transgenic mice expressing erGAP1. The expression of the biosensor was controlled by the ubiquitous promoter CAG-GS (31). Among the 12 transgenic lines obtained, 3 were selected based on their preferential expression in neural tissues. Transgenic mice were viable, developed and bred normally. The transgene was first visible at embryonic stage (E) E12-13 by GFP fluorescence, and expression remained stable until at least 18 mo, the oldest age tested. The Ca^{2+} sensor was robustly expressed in hippocampus, especially in pyramidal CA1 and CA2 areas and in dentate gyrus (Fig. 3 *A* and *B*). Expression was also strong in cortex and cerebellum, both in granule neurons and Purkinje cells (Fig. 3*C*). In all of the analyzed locations, erGAP1 was correctly expressed in the ER with no signs of aggregation.

To examine the functionality of the transgenic biosensor we first studied Ca^{2+} responses in single neurons dissociated from various neural tissues. This allows imaging fluorescence changes under better optical conditions. Cultured hippocampal transgenic neurons displayed a robust erGAP1 expression in ER, clearly visible in somata and dendrites (Fig. 3*D*). The probe was fully functional as demonstrated by the ratio changes in response to glutamate (15 ±1%, $n = 13$), 20 mM caffeine (25 ±1%, $n = 13$), or 50 mM caffeine (43 ±2%, $n = 13$) (Fig. 3*G*). The responses were rapid and reversible, and basal levels were rapidly recovered upon removal of stimuli. Similar changes were obtained in somata and dendrites (Fig. 3*G* and Movie S2).

We next examined the sensor signal in hippocampal slices isolated from erGAP1 mice. At low magnification the living slices showed an intense signal throughout the whole hippocampus (Fig. 3*E*). A close-up of the CA1 region showed the sensor distribution in individual pyramidal neurons (Fig. 3*F*). Functional responses are exemplified in Fig. 3*H*, where two consecutive caffeine pulses caused a decrease of the ratio (Fig. 3*H*, *Lower*) with reciprocal changes of F_{470} and F_{405} (Fig. 3*H*, *Upper*). The signal was reproducible and fully reversible upon stimulus removal. The average decrease of ratio in 42 cells (five mice) was 16.5 ± 0.5% (mean ± SEM).

A particularly robust fluorescence signal was observed in DRGs and spinal cord. In newborn DRG neurons the sensor was fully functional, as demonstrated by the two- to threefold ratio change upon maximal caffeine stimulation (Fig. S8*A*), that closely paralleled the results obtained in virally transduced DRGs (Fig. 2*F*). ER Ca^{2+} dynamics in transgenic erGAP1-expressing spinal motor neurons is shown in Fig. S8*B*. A strong and reversible effect of caffeine was observed in all of the motor neurons present in the field ($n = 10$). These results demonstrate that the sensor fully retained its features in the transgenic animal.

Discussion

We have developed a Ca^{2+} sensor family based on the fusion of two jellyfish proteins, GFP and aequorin. Unlike sensors based on bioluminescence or bioluminiscence resonance energy transfer (BRET) (32), GAP is a fluorescent protein that does not require reconstitution with cofactors. GAP is a ratiometric sensor with two excitation maxima (403 and 470 nm), at which fluorescence intensities change inversely upon Ca^{2+} binding. Ratiometric sensors are advantageous over single-wavelength ones, because ratioing can correct putative artifacts due to bleaching, focal-plane shifts, or other conditions that modify fluorescence similarly at the two wavelengths. The GAP fluorescence ratio changes about fourfold between Ca^{2+}-free and Ca^{2+}-saturated states.

Interestingly, the Hill coefficient for GAP1 has a value of 1, indicating that GAP Ca^{2+}-dependent fluorescence may involve only one functional EF hand. This contrasts with the two to three Ca^{2+} ions bound to aequorin when this is used as a bioluminescent probe (33). In this case, light emission requires oxidation of its cofactor coelenterazine. Different affinities for Ca^{2+} of the three EF sites and Ca^{2+} binding cooperativity between them explain the steep Ca^{2+} concentration dependence of aequorin. This means that when different regions with high or low Ca^{2+} content are monitored together, the average aequorin signal is heavily skewed toward the high-calcium level. Under similar conditions, GAP is advantageous and will report a more balanced average Ca^{2+} concentration. In addition, the nonexponential Ca^{2+} dependence of GAP makes its calibration easier.

Because GFP and aequorin are both from jellyfish, with no mammalian homologs, the possibility of interactions between GAP and mammalian partners is minimized. This makes GAP a truly orthogonal calcium indicator in contrast to the widely used calmodulin-based indicators. Aequorin has been extensively used, even at high concentrations, with no reports of disturbances by

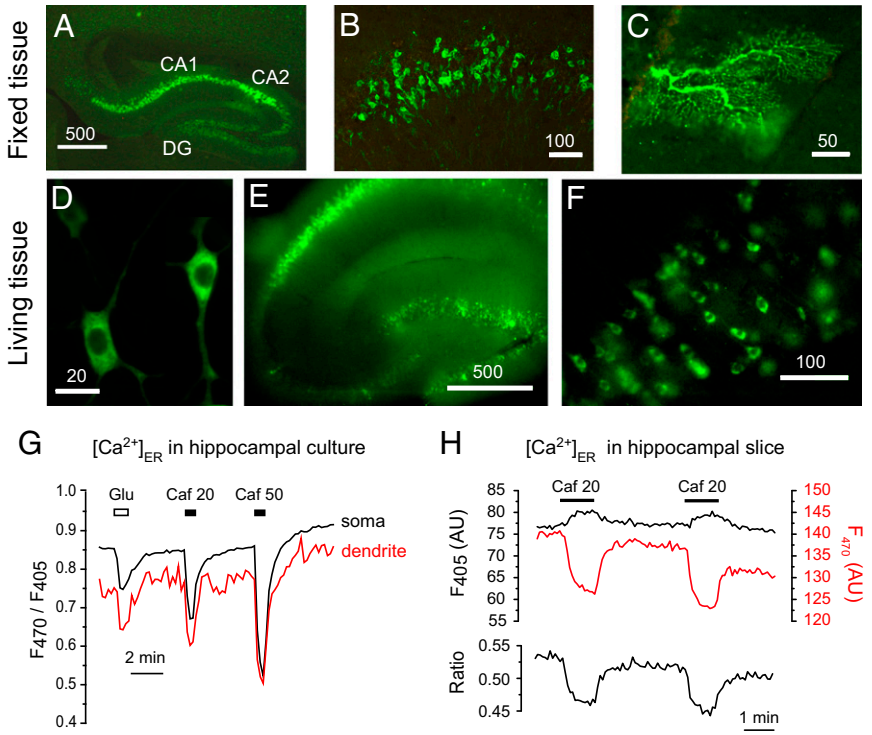

Fig. 3. Characterization of transgenic mice expressing erGAP1. (*A*) Fixed brain section showing erGAP1 expression in the hippocampus of a 6-wk–old mouse. Note the high level of expression in CA1 and CA2 regions and expression in dentate gyrus (DG). (*B*) Detail of CA1 hippocampal pyramidal cells showing high expression of erGAP1 in a 4-mo–old mouse. (*C*) Detail of a section through the cerebellum of a 8-mo–old mouse showing the dendritic tree of a Purkinje cell expressing erGAP1. (*D*) Two living pyramidal neurons expressing erGAP1 in primary culture; cells were isolated from the hippocampi of neonatal P0 mice and cultured for 9 d. (*E*) Low magnification image of a hippocampal slice (L20). (*F*) A close-up of the CA1 region. (*G*) Measurements of $[Ca^{2+}]_{ER}$ in the soma and dendrites of dissociated hippocampal neurons isolated from P2 mice and stimulated with glutamate (20 μM) or caffeine (20 and 50 mM). The images are shown in Movie S2. (*H*) Changes of erGAP1 fluorescence evoked by two consecutive caffeine (20 mM) pulses in a representative hippocampal slice isolated from a 1-mo–old transgenic mouse (L20). Individual wavelength fluorescence and ratio traces are shown. Traces are the average of nine neurons present in the same field.

binding to endogenous mammalian partners (21). In this study we demonstrate functional expression of GAP (or GAP1) in three systems: (*i*) transiently or stably expressing HEK293 or HeLa cells; (*ii*) virally infected or lipofectamine transfected primary neurons; and (*iii*) neuronal tissues of transgenic mice. In all cases the sensor was fully functional, and no signs of cellular perturbation were observed.

GAP fluorescence is pH-insensitive in the 6.2–8.2 range, which makes it particularly useful to image Ca^{2+} in nonneutral locations such as acidic Golgi apparatus or alkaline mitochondria. Both GAP and GAP1 are also insensitive to Mg^{2+}, which may circumvent putative artifacts due to differences in Mg^{2+} content among organelles and/or changes in Mg^{2+} concentration upon cell activation (34).

Effective Ca^{2+} measurements in distinct Ca^{2+} compartments require GECIs with customized Ca^{2+} affinity. We have reduced GAP affinity for Ca^{2+} to conform to the higher Ca^{2+} concentrations found in the Golgi apparatus or the ER. The mutant GAP1 displayed a 60-fold decrease of the affinity for Ca^{2+} whereas it retained the high dynamic range of GAP. Consequently, erGAP1 enabled monitoring $[Ca^{2+}]_{ER}$ changes upon stimulation either with $InsP_3$ agonists or with ryanodine receptor agonists such as caffeine. In agreement with previous data, GAP1 targeted to trans-Golgi apparatus showed that this organelle behaves as a high–Ca^{2+}-content store that can be discharged in response to $InsP_3$-producing agonists (11).

One of the main advantages of GECIs is their potential to selectively monitor $[Ca^{2+}]$ in subcellular compartments, although effective targeting is not always guaranteed. For example, ratiometric pericam is a reliable mitochondrial Ca^{2+} sensor (35), but is not functional in the ER. Here we demonstrate that GAP is targetable to a variety of organelles, including cytosol, nucleus, mitochondria, Golgi apparatus, or ER, and proved to be functional in all these locations. Moreover, the dual-excitation ratiometric probe erGAP1 fills a gap in the current collection of ER Ca^{2+} fluorescent indicators and complements other existing probes, such as the dual-emission ratiometric cameleon D1ER or the single-wavelength catchER. erGAP1 exhibits three- to fourfold larger responses than D1ER as demonstrated by a direct comparison between the performance of both sensors in HeLa cells or hippocampal neurons in response to the same stimuli (Fig. S5).

Another major application of GECIs is their potential to create transgenic organisms. However, the signal-to-noise ratio and the dynamic range of most of the transgenic biosensors is dramatically reduced in vivo. This has been explained by the use of FRET-based sensors with poor optical tissue penetration or by overexpression of endogenous proteins such as calmodulin (36). GAP is neither a FRET sensor, nor a mammalian-derived protein; thus it unlikely interacts with cellular partners. We have generated several lines of transgenic mice that stably and robustly express erGAP1 in neural tissues. In transgenic neurons, erGAP1 displayed a signal-to-noise ratio and a dynamic range comparable to virally delivered erGAP1 neurons. To our knowledge, the only other fluorescent Ca^{2+} ER sensor expressed in a transgenic mouse is the yellow cameleon YC3.3-er, specifically in pancreatic β-cells (37). Therefore, erGAP1 transgenic lines provide a useful tool to monitor ER calcium dynamics in neural tissues and can be used to study neurodegenerative disorders such as Alzheimer's disease, for which a "calcium hypothesis" has been proposed (38).

In summary, the GAP family of sensors provides a unique combination of the archetypical properties of a GECI: namely, dual-excitation ratioing, good signal-to-noise ratio, large dynamic

range, good photonic and thermal stability, pH- and Mg^{2+}-insensitivity, tunable Ca^{2+} affinity, targetability to organelles, and easy calibration. In addition, GAP is stably expressed in transgenic mice with robust performance and no signs of toxicity. This opens an avenue for studies of Ca^{2+} dynamics in vivo.

Materials and Methods

Detailed methods and any associated references are available in *SI Materials and Methods*.

Gene Construction. GFPuv was PCR-amplified from the pBAD-GFPuv plasmid (Clontech). GAP was engineered by fusing the C terminus of GFPuv and the N terminus of aequorin through the linker sequence TATPATTPTTAPTAGT. Low Ca^{2+} affinity GAP1 was generated by site-directed mutagenesis at positions D117A, D119A and D163A (aequorin).

Ca^{2+}, pH-, and Mg^{2+} Titration. GAPs cDNAs were cloned into the pET28A plasmid and transformed into *Escherichia coli* BL21 (Stratagene). Recombinant proteins with N-terminal poly-histidine tags were purified with Ni-Sepharose beads (GE Healthcare). GAP Ca^{2+} calibration was performed in MOPS/Tris buffers with different Ca^{2+} concentrations. Titration of pH was performed using a series of buffers with pH values ranging from 6.2 to 8.2. Mg^{2+} titration was done with solutions varying from 0.2 to 5 mM Mg^{2+}. GAP1 Ca^{2+} calibration was performed in situ in digitonin-permeabilized HeLa cells that stably expressed erGAP1.

Cell Culture and Transfection. HeLa and HEK293 cells were transfected with pcDNA3 expression vectors encoding different variants of GAP. Organelle targeting constructs were generated by in-frame fusion of GAP or GAP1 to the appropriate targeting sequence. HeLa cell lines stably expressing erGAP1 or goGAP1 were produced by lipofectamine transfection or electroporation, respectively.

Virus Production. erGAP1 was cloned into the pHSVpUC plasmid and Herpes Simplex Virus amplicons were generated.

Transgenic Mice. erGAP1 cDNA was subcloned into the pCAG-GS expression vector and injected into B6CBAF2 fertilized eggs. The transgene was detected in 12 lines by quantitative-PCR. Lines 11, 20 and 30 were further examined due to their preferential expression in neural tissues.

Ca^{2+} Imaging. Dual-excitation imaging of GAP-expressing monolayer cultures or acute hippocampal slices was performed in a fluorescent microscope equipped with 403 and 470 nm excitation filters (emission above 520 nm).

ACKNOWLEDGMENTS. We thank M. García and J. Fernández for their technical assistance; I. López and Y. Gaciño for assistance with mice; A. Martín for assistance in cell sorting; M. Rodriguez for assistance with spinal cord motoneurons isolation; M. Torres and L. M. Criado for mouse microinjections; L. Looger for providing the pCAG plasmid; J. Llopis for the GT-YFP plasmid; R. Tsien for the D1ER plasmid; J. Yang for catchER plasmid; R. Soler for introducing us to the motoneuron cultures; and F. Perocchi, T. Oertner, and T. Schimmang for suggestions on the manuscript. This work was supported by grants from the European Research Area Net (ERA-Net) program, the Spanish Ministerio de Economia y Competitividad (SAF2008-03175-E, BFU2010-17379), and the Instituto de Salud Carlos III (RD06/0010/0000).

1. Clapham DE (2007) Calcium signaling. *Cell* 131(6):1047–1058.
2. Feske S (2007) Calcium signalling in lymphocyte activation and disease. *Nat Rev Immunol* 7(9):690–702.
3. Rizzuto R, Pozzan T (2006) Microdomains of intracellular Ca2+: Molecular determinants and functional consequences. *Physiol Rev* 86(1):369–408.
4. Hofer AM, Machen TE (1993) Technique for in situ measurement of calcium in intracellular inositol 1,4,5-trisphosphate-sensitive stores using the fluorescent indicator mag-fura-2. *Proc Natl Acad Sci USA* 90(7):2598–2602.
5. Shimomura O (1995) A short story of aequorin. *Biol Bull* 189(1):1–5.
6. Llinás R, Blinks JR, Nicholson C (1972) Calcium transient in presynaptic terminal of squid giant synapse: Detection with aequorin. *Science* 176(4039):1127–1129.
7. Inouye S, et al. (1985) Cloning and sequence analysis of cDNA for the luminescent protein aequorin. *Proc Natl Acad Sci USA* 82(10):3154–3158.
8. Rizzuto R, Simpson AW, Brini M, Pozzan T (1992) Rapid changes of mitochondrial Ca2+ revealed by specifically targeted recombinant aequorin. *Nature* 358(6384):325–327.
9. Montero M, et al. (1995) Monitoring dynamic changes in free Ca2+ concentration in the endoplasmic reticulum of intact cells. *EMBO J* 14(22):5467–5475.
10. Brini M, et al. (1993) Nuclear Ca2+ concentration measured with specifically targeted recombinant aequorin. *EMBO J* 12(12):4813–4819.
11. Pinton P, Pozzan T, Rizzuto R (1998) The Golgi apparatus is an inositol 1,4,5-trisphosphate-sensitive Ca2+ store, with functional properties distinct from those of the endoplasmic reticulum. *EMBO J* 17(18):5298–5308.
12. Mitchell KJ, et al. (2001) Dense core secretory vesicles revealed as a dynamic Ca(2+) store in neuroendocrine cells with a vesicle-associated membrane protein aequorin chimaera. *J Cell Biol* 155(1):41–51.
13. Rudolf R, Mongillo M, Rizzuto R, Pozzan T (2003) Looking forward to seeing calcium. *Nat Rev Mol Cell Biol* 4(7):579–586.
14. Tang S, et al. (2011) Design and application of a class of sensors to monitor Ca2+ dynamics in high Ca2+ concentration cellular compartments. *Proc Natl Acad Sci USA* 108(39): 16265–16270.
15. Miyawaki A, et al. (1997) Fluorescent indicators for Ca2+ based on green fluorescent proteins and calmodulin. *Nature* 388(6645):882–887.
16. Kotlikoff MI (2007) Genetically encoded Ca2+ indicators: Using genetics and molecular design to understand complex physiology. *J Physiol* 578(Pt 1):55–67.
17. Whitaker M (2010) Genetically encoded probes for measurement of intracellular calcium. *Methods Cell Biol* 99:153–182.
18. Palmer AE, Tsien RY (2006) Measuring calcium signaling using genetically targetable fluorescent indicators. *Nat Protoc* 1(3):1057–1065.
19. Rogers KL, et al. (2007) Non-invasive in vivo imaging of calcium signaling in mice. *PLoS ONE* 2(10):e974.
20. Yamano K, et al. (2007) Identification of the functional expression of adenosine A3 receptor in pancreas using transgenic mice expressing jellyfish apoaequorin. *Transgenic Res* 16(4):429–435.
21. Webb SE, Rogers KL, Karplus E, Miller AL (2010) The use of aequorins to record and visualize Ca(2+) dynamics: From subcellular microdomains to whole organisms. *Methods Cell Biol* 99:263–300.
22. Manjarrés IM, et al. (2008) Red and green aequorins for simultaneous monitoring of Ca2+ signals from two different organelles. *Pflugers Arch* 455(5):961–970.
23. Crameri A, Whitehorn EA, Tate E, Stemmer WP (1996) Improved green fluorescent protein by molecular evolution using DNA shuffling. *Nat Biotechnol* 14(3):315–319.
24. Gorokhovatsky AY, et al. (2004) Fusion of Aequorea victoria GFP and aequorin provides their Ca(2+)-induced interaction that results in red shift of GFP absorption and efficient bioluminescence energy transfer. *Biochem Biophys Res Commun* 320(3):703–711.
25. Chamero P, et al. (2008) Nuclear calcium signaling by inositol trisphosphate in GH3 pituitary cells. *Cell Calcium* 43(2):205–214.
26. Alonso MT, García-Sancho J (2011) Nuclear Ca(2+) signalling. *Cell Calcium* 49(5):280–289.
27. Palmer AE, Jin C, Reed JC, Tsien RY (2004) Bcl-2-mediated alterations in endoplasmic reticulum Ca2+ analyzed with an improved genetically encoded fluorescent sensor. *Proc Natl Acad Sci USA* 101(50):17404–17409.
28. Kendall JM, Dormer RL, Campbell AK (1992) Targeting aequorin to the endoplasmic reticulum of living cells. *Biochem Biophys Res Commun* 189(2):1008–1016.
29. Montero M, Barrero MJ, Alvarez J (1997) [Ca2+] microdomains control agonist-induced Ca2+ release in intact HeLa cells. *FASEB J* 11(11):881–885.
30. Llopis J, McCaffery JM, Miyawaki A, Farquhar MG, Tsien RY (1998) Measurement of cytosolic, mitochondrial, and Golgi pH in single living cells with green fluorescent proteins. *Proc Natl Acad Sci USA* 95(12):6803–6808.
31. Tian L, et al. (2009) Imaging neural activity in worms, flies and mice with improved GCaMP calcium indicators. *Nat Methods* 6(12):875–881.
32. Jiang LI, et al. (2007) Use of a cAMP BRET sensor to characterize a novel regulation of cAMP by the sphingosine 1-phosphate/G13 pathway. *J Biol Chem* 282(14):10576–10584.
33. Head JF, Inouye S, Teranishi K, Shimomura O (2000) The crystal structure of the photoprotein aequorin at 2.3 A resolution. *Nature* 405(6784):372–376.
34. Szanda G, Rajki A, Gallego-Sandín S, Garcia-Sancho J, Spät A (2009) Effect of cytosolic Mg2+ on mitochondrial Ca2+ signaling. *Pflugers Arch* 457(4):941–954.
35. Nagai T, Sawano A, Park ES, Miyawaki A (2001) Circularly permuted green fluorescent proteins engineered to sense Ca2+. *Proc Natl Acad Sci USA* 98(6):3197–3202.
36. Palmer AE, Qin Y, Park JG, McCombs JE (2011) Design and application of genetically encoded biosensors. *Trends Biotechnol* 29(3):144–152.
37. Hara M, et al. (2004) Imaging endoplasmic reticulum calcium with a fluorescent biosensor in transgenic mice. *Am J Physiol Cell Physiol* 287(4):C932–C938.
38. LaFerla FM (2002) Calcium dyshomeostasis and intracellular signalling in Alzheimer's disease. *Nat Rev Neurosci* 3(11):862–872.